

AD\_\_\_\_\_

Award Number: W81XWH-05-1-0101

TITLE: Development and Evaluation of Sterographic Display for Lung Cancer  
Screening

PRINCIPAL INVESTIGATOR: Xiao Hui Wang, M.D., Ph.D.  
Walter F. Good  
Carl R. Fuhrman  
Howard E. Rockett  
David Gur

CONTRACTING ORGANIZATION: University of Pittsburgh  
Pittsburgh, PA 15260

REPORT DATE: December 2005

TYPE OF REPORT: Annual

PREPARED FOR: U.S. Army Medical Research and Materiel Command  
Fort Detrick, Maryland 21702-5012

DISTRIBUTION STATEMENT: Approved for Public Release;  
Distribution Unlimited

The views, opinions and/or findings contained in this report are those of the author(s) and should not be construed as an official Department of the Army position, policy or decision unless so designated by other documentation.

REPORT DOCUMENTATION PAGE				Form Approved OMB No. 0704-0188	
Public reporting burden for this collection of information is estimated to average 1 hour per response, including the time for reviewing instructions, searching existing data sources, gathering and maintaining the data needed, and completing and reviewing this collection of information. Send comments regarding this burden estimate or any other aspect of this collection of information, including suggestions for reducing this burden to Department of Defense, Washington Headquarters Services, Directorate for Information Operations and Reports (0704-0188), 1215 Jefferson Davis Highway, Suite 1204, Arlington, VA 22202-4302. Respondents should be aware that notwithstanding any other provision of law, no person shall be subject to any penalty for failing to comply with a collection of information if it does not display a currently valid OMB control number. <b>PLEASE DO NOT RETURN YOUR FORM TO THE ABOVE ADDRESS.</b>					
1. REPORT DATE (DD-MM-YYYY) 01-12-2005		2. REPORT TYPE Annual		3. DATES COVERED (From - To) 8 Nov 2004 – 7 Nov 2005	
4. TITLE AND SUBTITLE Development and Evaluation of Sterographic Display for Lung Cancer Screening				5a. CONTRACT NUMBER	
				5b. GRANT NUMBER W81XWH-05-1-0101	
				5c. PROGRAM ELEMENT NUMBER	
6. AUTHOR(S) Xiao Hui Wang, M.D., Ph.D.; Walter F. Good; Carl R. Fuhrman; Howard E. Rockett; David Gur;  E-mail: xwang@mail.magee.edu				5d. PROJECT NUMBER	
				5e. TASK NUMBER	
				5f. WORK UNIT NUMBER	
7. PERFORMING ORGANIZATION NAME(S) AND ADDRESS(ES)  University of Pittsburgh Pittsburgh, PA 15260				8. PERFORMING ORGANIZATION REPORT NUMBER	
9. SPONSORING / MONITORING AGENCY NAME(S) AND ADDRESS(ES) U.S. Army Medical Research and Materiel Command Fort Detrick, Maryland 21702-5012				10. SPONSOR/MONITOR'S ACRONYM(S)	
				11. SPONSOR/MONITOR'S REPORT NUMBER(S)	
12. DISTRIBUTION / AVAILABILITY STATEMENT Approved for Public Release; Distribution Unlimited					
13. SUPPLEMENTARY NOTES					
14. ABSTRACT The main purpose of this project is to investigate the feasibility and efficacy of using a stereo display workstation for lung cancer screening on CT images. The tasks included in this project are development and evaluation of stereo image projection and display for chest CT images, observer performance evaluation for the stereo display, and stereo feature analysis and comparison to the conventionally used display methods for lung cancer detection. During this progress period, we have made progress in following tasks. 1. Building stereo display workstation for chest CT images: we have investigated effects of several commonly used compositing methods on nodule representation and detection in stereo CT images. Among these methods, conventional maximum intensity projection (MIP) produced the highest image contrast, but gave ambiguities in local geometric detail and texture, whereas averaging compositing resulted in the lowest contrast, but preserved geometric details. Distance-weighted MIP partially recovered geometric information, which was lost in images composited by conventional MIP. 2. Preparing cases for observer performance study: to get consensus truth of the cases collected for this project, three radiologists have read the cases and recorded their subjective ratings on conventional workstation. Inter- and intra-reader variations have been calculated, and will be compared with the readings from stereo display. 3. Conducting pilot observer performance study: six radiologists have participated a pilot observer performance study. The study has three display modes, conventional slice-by-slice mode, conventional MIP display mode and stereo display mode. The performance of lung nodule detection and characterization are examined and compared for the three modes.					
15. SUBJECT TERMS lung cancer screening, stereo display, volumetric rendering, observer performance study					
16. SECURITY CLASSIFICATION OF:			17. LIMITATION OF ABSTRACT	18. NUMBER OF PAGES	19a. NAME OF RESPONSIBLE PERSON
a. REPORT	b. ABSTRACT	c. THIS PAGE			USAMRMC
U	U	U	UU	28	19b. TELEPHONE NUMBER (include area code)

## Table of Contents

Cover.....	1
SF 298.....	2
Introduction.....	4
Body.....	4
Key Research Accomplishments.....	11
Reportable Outcomes.....	11
Conclusions.....	12
References.....	12
Appendices.....	14

## INTRODUCTION

Lung cancer is a leading cause of death in the United States [1,2]. The results from several large lung cancer screening studies indicate that early detection and treatment can reduce mortality rate in most types of lung cancer cases [3-6]. Currently, low-dose CT scanner is a primary tool used for lung cancer screening. For each screening case, a set of image slices covering entire lung area is generated and viewed on workstation monitors. Despite of 3D data obtained from CT scanner, the conventional reading method for lung CT image interpretation is to read images slice-by-slice. This reading method requires radiologists to mentally reconstruct images in 3D space from a set of 2D images to differentiate normal tubular structures from nodules. Furthermore, with improved technology for CT scanner, higher resolution images produce more images per scan, which eventually will exceed radiologists' ability to read cases in slice-by-slice mode. The need of 3D data presentation of CT images has become crucial for ever-increasing numbers generated from CT scanner and for improvement of radiologists' performance on image data interpretation. We have proposed to develop a stereo display workstation for reading lung CT images. Stereopsis is the mechanism used in human vision system to perceive objects in our three dimensional space. The 3D display using stereoscopic projection should produce a natural and efficient solution for 3D data presentation. In this proposal, we hypothesized that the efficacy of lung cancer screening, by CT scanner, can be increased by use of a suitable designed stereoscopic display. Specifically, we expect that both efficiency, and accuracy for the detection of lung nodules, will be increased significantly over what can be achieved when reading cases in currently used display modes. To achieve the goals in this proposal, we have specified our aims in:

- 1) Develop and integrate the hardware and software required to implement a stereoscopic display tailored to chest CT images.
- 2) Use a subset of lung cancer cases, verified either by pathology or by followup, to evaluate the display system.
- 3) Perform a retrospective study to measure relative accuracy and reading efficiency, for detection and classification of lung nodules, between three display modes including stereoscopic 3D mode from this project, and other two commonly used modes, slice-by-slice and maximum-intensity-projection thick slice.

## BODY

### **Integrate Hardware (task 1)**

To implement the stereo display workstation, certain requirements of hardware components and hardware constructions need to be fulfilled before integration of the hardware and software for viewing stereographs.

The integrated hardware for stereo display consisted of a PC computer equipped with stereographic card, a programmable keypad, a monitor, a signal synchronizer, and a shutter glasses.

*Computer* — A 2.8 GHz AMD Athlon 64 personal computer was configured for stereo image processing and stereographic display. The computer has 3 hard disk units connected via RAID technology to create maximal disk capacity of 400 GH that can support massive data computing and real-time display for stereo chest CT workstation. The NVIDIA Quadro FX1100 graphic card installed in the computer is stereo capable that provides display buffers and OpenGL/DirectX support necessary for stereographic presentation. The computer's performance and stereographic capability was tested for the optimal level to the tasks in this project.

*Keyboard* — Several functionalities for controlling stereo display window were encoded into a programmable keypad. The key-controlled features include, but not limited to, adjusting window/level settings, scrolling sequential images in a case, changing number of image slices that are used for composing stereo images, and toggling markers used for detected nodule. In lieu of regular keyboard, the keypad we reconstructed is tempered to the needs of lung nodule detection and classification in the stereo display. By simply pushing on the functional keys, radiologists can manage the display to the level of optimal viewing and task specific.

*Stereo output* — Three parts, monitor, signal emitter and shutter glasses, in the integrated hardware are mainly responsible for stereo image output. In order to perceive stereoscopic view of the images, left and right images need to be viewed separately by each of corresponding eyes at frame rate of at least 60 HZ for each eye. The graphic card was configured to alternate displayed left and right images and output the signal through the emitter to synchronize

the shutter glasses to the refresh cycle of the monitor. The monitor with refresh rate of 144 HZ is used to give flicker-free stereo images viewed through shutter glasses.

### **Develop 3D Geometric Projection Algorithms and Transparency-Contrast Models (tasks 2, 3)**

Display a 3D chest CT dataset in stereo requires that two 2D projections, corresponding to left and right eye views (stereo pair), be performed. Projection methods consist of geometric projection model and illumination model. The interaction between geometric projection model, illumination model and optical characteristics at each voxel can be integrated along rays to calculate the values of pixels on 2D projection. For CT images, it is customary, for display, to assign brightness values having a monotonic, but nonlinear relationship to X-ray attenuation coefficients, as measured in Hounsfield units. In keeping with this, we assumed that each CT voxel has a neutral color (some shade of gray) and a brightness value that is some affine mapping of its Hounsfield value, with pixels corresponding to low X-ray attenuation appearing as darker intensities and pixels corresponding to higher X-ray attenuation appearing brighter.

In stereopsis, contrast is important for depth perception [7-8], and subjective evaluations from our studies indicate that optimization of local contrast is necessary for detecting fine structures in stereo displays of chest CT data. Monocular occlusions from the perspective transformation and from averaging effects of transparency models incorporated in traditional volumetric reconstruction algorithms possibly reduces contrast in the reconstructed stereo pairs with increased image depth from stacks of CT slices. Our goal, therefore, was to maximize the detectability of nodules, but at the same time, maintain sufficient geometric fidelity to allow detected nodules to be accurately characterized. The issues of clearly displaying other structures of interest such as vessels, bronchi and bone and incorporation of monoscopic depth cues were also addressed and implemented in the study.

#### *a. Geometric Models*

The two geometric projection models that are relevant in the context of this application are the orthographic and the perspective transformations. Orthographic projection, which is used by traditional Maximum Intensity Projection (MIP), is not compatible with realistic stereographic projection. Perspective transformations have been used to a limited extent in the medical environment [9], but their added complexity is not always justified for monoscopic viewing. Geometric perspective is one of the more important monoscopic depth cues when familiar scenes are being viewed, though the extent, to which it will be of value for viewing the interior of lungs, is not known.

To test the prospective use of perspective transformation for stereo view of lung images, we applied perspective transformation in stereo image compositing algorithm to a set of chest CT images. We assumed that the topmost slice being displayed is the same distance as the screen of the physical display, the viewing distance between a viewer and the screen is 45-cm, and the interocular distance is 6.5-cm. We have maintained these conditions throughout this work, but in our studies we found that stereoscopic convergence is not appreciably affected by the exact seating position — as long as the eyes are maintained level relative to the monitor.

It is generally aware that volumetric lung images acquired by current CT systems have different resolutions in the axial direction than in planes perpendicular to that direction. The axial resolution is more a function of the user's specification to the reconstruction algorithm, than to the acquisition protocol. The anisotropic nature of the dataset (e.g., voxels are typically  $0.7\text{-mm} \times 0.7\text{-mm} \times 2.5\text{-mm}$ ), and our choice of a non-orthogonal projection, necessitates resampling the data to obtain the actual values used in ray casting. The most common method used for interpolation in computer graphics is trilinear interpolation because it is easy to implement, computationally efficient and comparable to other more sophisticated interpolation methods in terms of visual effect. We used trilinear interpolation to resample the data and insert effectively the virtual slices between each pair of real slices to achieve final pixel dimension close to isotropic.

The results from MIP volumetric rendering with perspective transformation produced stereo images that had true 3D depth and spatial differentiation of interior lung structures. Comparing visually to perspective transformation, MIP rendering with orthogonal transformation generated only monoscopic 3D view and no information of depth or of the geometrical relationships between structures. However, further quantitative comparison of these two transformations and their utility in medical image diagnosis, chest CT in particular in our case, will be performed in the upcoming observer performance studies (year two).

### b. Implement monoscopic depth cues

Disparity between stereoscopic views is the primary depth cue being studied in this work. However, there exist monoscopic depth cues that greatly assist viewers in achieving stereopsis, and it is desirable to include these cues, to the extent they are not in conflict with the goal of optimizing radiographic interpretation. Two monoscopic cues were incorporated in the stereo compositing methods, geometric depth cues and brightness cue.

**Geometric cues** — The main geometric depth cue we have included was geometric perspective which, as was discussed above, was the transformation adopted exclusively for rendering stereoscopic images in this project. A second geometric cue we have included was the occlusion of voxels by intervening structures to determine the amount of illumination projected on display plane for an object.

**Brightness cue** -- We have modeled brightness variation with respect to depth change. To model a systematic reduction in brightness values with increasing depth or distance, we assumed that each slice has a fixed optical density that reduces the brightness of slices lying behind it. In the actual implementation, each slice was assumed to have the same fixed optical density and weighing factors, derived from a geometric sequence, was applied so as to achieve a ratio of weights,  $K$ , between the back slice and the front slice. For  $N$  slices, and assuming the total of all weights equals 1, the weights  $W_i$ ,  $i=0, \dots, N-1$ , was calculated as follows:

$$W_i = \frac{1 - K^{\frac{1}{N-1}}}{\frac{N}{1 - K^{\frac{1}{N-1}}}} K^{\frac{i}{N-1}}$$

In the case of our distance-weighted MIP projections, the front slice weight was 1, and the sum was irrelevant. In our preliminary studies we found that  $K=0.5$  provides a reasonable indication of depth without excessively reducing the brightness of the deeper slices.

### c. Illumination Models

Volume rendering, which was adopted for our stereo image compositing, attempts to identify and classify all voxels of an object, and to assign optical properties (e.g., transparency, color and brightness) to each voxel and is particularly useful in applications, such as chest CT, where the structures of interest are rather sparsely distributed.

The challenging task in volume rendering is to develop an optimal brightness / contrast / transparency model for assigning optical characteristics to each rendered voxel. Because the intrinsic property being imaged with CT is actually X-ray attenuation coefficient, the assignment of optical properties to CT voxels is entirely artificial and should be done in a manner that best facilitates the interpretation of the image data. Two illumination models that are suitable for chest CT data have been examined and compared.

1. **Averaging model** — this compositing method that is commonly applied in volume rendering averages voxel values along rays and effectively reduces the contrast of smaller objects, which may appear in only a few slices, as the displayed volume is increased by adding slices. Nevertheless, volume rendering with averaging does preserve spatial information such as textures and local geometry.

For chest CT images, instead of simply averaging voxel values along rays, we adopted a light emission / transmission / occlusion model that assumed that each voxel emits light in proportion to its brightness when CT images are displayed at a normal window and level for nodule detection and that uses distance information (distance-weighting factors) to determine the amount of this emitted light that reaches the projection plane (appendix A). Specifically, it was assumed that each slice has a fixed optical density that decreases the brightness of slices lying behind it. The total of all distance weights was equal to one. The ratio of weights between the last (the slice with the largest distance from screen) and first slice (the slice at screen level) controls the level of transparency for a given volume.

We studied a range of these ratios for lung CT images and empirically set the ratio to 0.5 to achieve a balance between the use of brightness weighting as a depth cue and visibility of the back slice. The final value for a voxel is the sum of distance-weighted pixel values in a perspective transformation ray.

2. MIP models — by using the maximum pixel intensity along each ray of the projection, MIP is designed to maximize contrast in situations where sparsely distributed objects are being viewed against a dark background, which is the situation that occurs in projecting thick volumes of the lung. Its main deficiency is that it does not preserve local spatial structure such as texture and local geometry. This is because a bright pixel appearing in a view for one eye will not necessarily have a corresponding bright pixel that appears in the view for the opposite eye.

In our stereographic compositing with MIP principle, we have experimented two different ways of applying MIP compositing. First, we used a perspective projection in which the maximum value along each ray was used as the projected value. As we mentioned above, this approach generally is not possible for an observer's vision system to unambiguously match corresponding points between the two views because the projected voxels may be different between the stereo views. In practice, we found that the ambiguity in matching corresponding points between views primarily affects fine detail and does not interfere with the detection of objects composed of large clusters of bright voxels, although the exact shapes of these objects cannot be determined unambiguously.

In an attempt to incorporate a geometric cue common in traditional stereo projection methods, but also preserve the contrast advantage of MIP, we in turn used a perspective projection in which the maximum along each ray has been weighted, based on distance. The maximum (nearest) and minimum (farthest) weights were determined empirically, and weights for slices between the first and last were calculated by using a geometric sequence, assuming a fixed optical density for each slice.

#### d. Compare compositing methods for lung nodule detection and characterization on stereo CT images

We compared averaging, MIP and distance-weighted MIP applied to various lung nodule types, sizes, and locations. MIP and distance-weighted MIP produced higher local contrast than compositing by averaging. Unlike averaging methods, which sacrifice contrast to take account of each voxel in a volume, the conventional MIP method is able to retain contrast in cases in which the object being viewed includes voxels that are brighter than the superimposed tissue. Applied to the task of lung nodule detection, despite a lack of geometric fidelity, conventional MIP images generally produce high local contrast that separates a nodule from its background and therefore enhances detection performance.

However, improvements in nodule visibility with the MIP method do not apply in certain cases in lung CT images. For a nodule to be detected with conventional MIP, it must contain some voxels that are brighter than its background. The case of a nodule overlying a rib is a particular concern, although it occurs relatively infrequently in projections of axial slabs unless the nodule is very close to a rib or the slab being viewed is relatively thick. Most voxels in such a nodule will not be as bright as voxels in the rib, and the nodule may be almost invisible.

One benefit of the distance-weighted MIP projection is that it can decrease the brightness of the background. As the position of a slab is changed, relative brightness weighting factors between voxels at different axial positions will change, and, in many instances, there will be an axial position at which a nodule will appear brighter than a rib, which can increase the likelihood that an obscured nodule becomes visible. Our results indicate that distance-weighted MIP partially recovered geometric information lost in conventional MIP by incorporating a distance cue into the compositing, and at the meantime, distance-weighted MIP had image contrast nearly equivalent to that produced by the conventional MIP method.

In addition to detection, nodule characteristics are essential and critical for clinically differentiating benign for malignant. Although conventional MIP is superior for detection, it was outperformed by the averaging method in terms of characterization. When comparing the three compositing methods visually for nodule characterization, the spiculated nodule border is clearly visible in stereo pairs composited with the averaging method, whereas this characteristic is not preserved in some of the stereo pairs composited with the conventional MIP method, especially those composited from thicker slabs. Distance-weighted MIP partially overcomes the problem of conventional MIP, and spiculated borders are still visible in the thicker slabs. For the smooth border of a nodule, we observed a similar

phenomenon. The geometric relationship is well presented with gradient changes in intensities along the smooth border of the nodule in the stereo pair composited with the averaging method. The same nodule is shown with lack of geometric fidelity in the stereo pair composited with conventional MIP. The lack of fidelity in module shape and geometric representation in conventional MIP images are attributed to the nature of MIP compositing, in which the two views may be based on projections of different voxels. Conversely, the averaging method is shown in this study to faithfully retain the characteristics of the nodules, including structural, spatial, and geometric information.

#### e. Test combinations of MIP and averaging

Each compositing method as described above has a particular balance of advantages and disadvantages, and may be optimal in certain situations but inappropriate for others. Based on our preliminary results, we believe that two rendering modes will need to be available to viewers – one optimized for nodule detection and one optimized for nodule characterization. Thus, in practice, it may actually be advantageous to view a volume with a range of compositing methods.

Because MIP appears to be best for nodule detection, and some form of voxel averaging is best for characterizing detected nodule, we have implemented and used two separate rendering methods, i.e. distance-weighted MIP and averaging, in a single stereoscopic display mode. The intention is that after a nodule has been detected in the distance-weighted MIP, the thickness of the displayed volume can be adjusted to include only slices that contain the nodule, and this volume can be displayed by using an averaging compositing method so the nodule can be characterized more accurately.

### **Write Display Software (task 4)**

The display software provided for the stereo viewing has been developed in the current progress period. The functionalities built into the software enabled readers to have real-time interaction with slice navigation through entire lung sections, to change viewing thickness of lung sections, and to adjust brightness / contrast of displayed images (Appendix B).

#### a. Write user interface

The display software was written as a Windows application implemented specifically with Win32 including MFC (Microsoft Foundation Classes), and SGI (Silicon Graphics Inc.) OpenGL (Open Graphics Library) language. The Windows API provided Windows framework and functional utilities of the user interface. The OpenGL functions enabled stereographic display by manipulating display functions on graphic processing unit. A typical user interface is shown in figure 1.

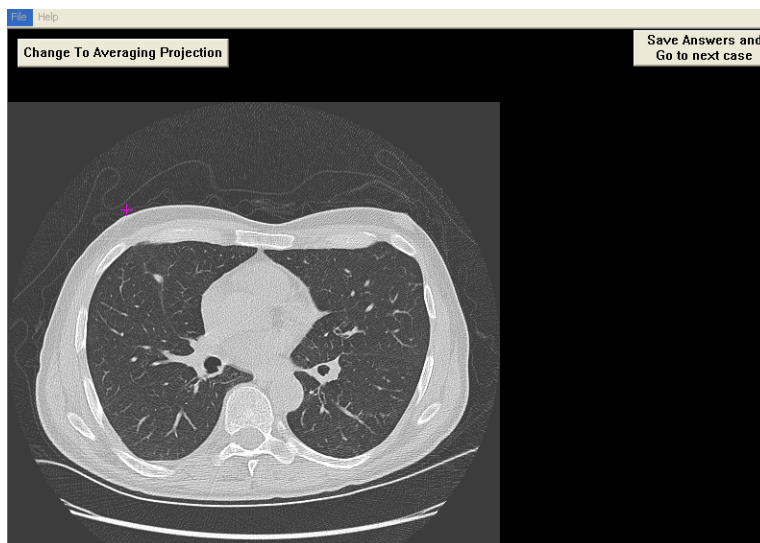


Figure 1. Window-based user interface.

projections

#### b. Write routines for prestaging

In order to have users to control the thickness (i.e., number of slices in a slab) and the axial position of stacks of 2D CT slices, all projections were precalculated and stored on the display's hard disk. For each case, the files were organized into a two-dimensional linked list that allows projections to be accessed by thickness and axial position in real-time. Software was written to render stereo image pairs from the CT data by the stereo projection algorithms described in tasks 2, 3.

For the comparisons, the software also included rendering traditional monoscopic MIP images. To be consistent with commercially available CT displays, monoscopic MIP images were generated using a standard orthogonal projection. The slice-by-slice display mode required only minimal additional software because, by design, this mode is actually a limiting case (i.e., volume thickness = 1 slice) of both the MIP and stereo modes.

All computer code was written in C++ language and tested thoroughly prior to its use in this study.

c. Write routines for window/level control

Window / level (contrast / brightness) mechanism was built into the display workstation with a default setting of 2000 / -500-HU for lung CT images. Real-time adjustment of window / level was enabled through encoded keys on the keypad.

d. Write routines for control of slice thickness and axial position

To achieve real-time performance in changing axial position in the CT volume and in changing the thickness of the displayed volume, stereo pairs corresponding to all admissible combinations were precalculated, organized into a 2D linked list, and stored on the hard drive. This required approximately 1-GB of disk storage per case, but was able to achieve nearly instantaneous response to changes in axial position or slice thickness.

**Write Software Needed To Perform Study (task 6)**

In the main study as well as the pilot study, readers are required to identify possible nodules and then characterize the detected nodules in three display modes. A software was written to implement functions required for the study, which include management of study cases and display modes, case randomization, electronic scoring of detected nodules, scaled onscreen ruler for nodule measurement, markers for detected nodules, and data archive. All implementations were written in C++ language and have been tested rigorously to meet the specifications of the study.

a. Write 3D cursor routine for making nodule locations

We were able to make a stereo cursor corresponding to the perspective view of displayed volume. In specific, the cursor can be specifically placed at a particular location in the 3D volume space. The size of the cursor is properly transformed to reflect the size perceived at a distance based on the spatial location of the cursor in the volume. With the stereo cursor, a reader can mark a nodule location (with 3 axes of x, y, and z) in the volume. At the present, we have placed the cursor in the middle of the viewing slab. To make a navigable stereo cursor, we just need to encode mouse wheel with the stereo cursor routines, since all the mechanisms have been laid out.

Besides serving as a location indicator, the stereo cursor was also made as an onscreen measure for nodule size. Horizontal or vertical line of the cursor represents unit of length that can be used for size approximation when the cursor is placed over a structure.

b. Implement case randomization

In observer performance study, case randomization is a procedure to assure that a reader's response is not biased by the order and the time of the cases presented. Our randomization routines were designed to generate random case list, remove the cases that have been examined and then present the cases for each reader at each reading session. Because of the multiple modes we need to test in this study, the randomization routines have also implemented function that checks status of a case across the modes.

c. Record findings

Electronic scoring form was implemented in the study software. When a reader clicks on a possible nodule, a scoring form with study questions will show on the screen. The questionnaire can be answered in the form of either check boxes or radio buttons. The answers as well as nodule's location will be saved after reader finishes scoring or will be neglected if reader chooses to delete the answers. A detected nodule is toggled with a marker and on/off states of the marker can be controlled at reader's will.

#### d. Write routines for monitoring readers' reading patterns

It is our intention to incorporate routines into the study software for keeping track of moves made by readers during case study. This data will be a part of evaluation criteria for the display study as well as be valuable reference for understanding psychophysical attributes in different display designs. During a reading session, the computer will periodically (at the rate of every 5<sup>th</sup> millisecond) record reading status, including anatomic location of displayed slice, displayed slice volume in the case of stereo or MIP mode, indication of status between observing case and scoring nodule, and indication of compositing methods between averaging and MIP in the case of stereo mode.

#### **Case Selection (task 7)**

The images selected for developing and evaluating the display were from subjects who have previously been scanned as part of the Pittsburgh Lung Cancer Screening Study, an ongoing lung cancer screening trial in our facility, of subjects that are considered be at high risk due to age and smoking history. The cases were acquired from a helical CT scanner (LightSpeed Plus, GE Medical Systems, Milwaukee, WI) with slices reconstructed at a thickness of 2.5-mm, which resulted in the production of, on average, 100 slices per case. The images were post-processed with a kernel convolution algorithm using GE standard software, to adjust image sharpness to be suitable for viewing lung tissue.

The cases we selected were from a population where lung nodules, of which most are noncancerous, are prevalent due to subjects' age and smoking history. The average number of nodules per case is about five. The actual distribution of nodules in our cases produces a somewhat lower sensitivity, for case-based analysis, than we were expecting. The high probability of finding positive cases would provide low sensitivity and less statistical power for comparing radiologists' performance of nodule detection across the different display modes, if we conduct case-based comparison study. To enhance the analytical power of the data, we will adopt an observation-based strategy as the primary method of analysis. That is, the performance will be analyzed based on each finding in a case and analyzed by FROC methods. The change in emphasis from a case-based study to an observation-based study means a significant increase in statistical power.

Meanwhile, we have included more readers in both the pilot study and the main study. Particularly, we have more readers, especially recruiting fellows, so as to reflect a spectrum of various levels of clinical experience of readers. This is an important issue for us, as we need to know if any performance change has any association with subjects' experience and, to the less extent, subjects' physical conditions (such as age, visual conditions), typically when stereoscopic vision and eyewear are involved in the study. The number of readers is increased from 3 to 6 in the pilot study, and from 6 to 8 in the main study. This increase of the number of readers gives further justification of reducing the number of cases we initially proposed.

As stated above, redefining the definition of study instance and adjusting reader structure allow achieving at least the same analysis power but fewer cases. As the result of that, the final number of cases we collected for this project is reduced to 290, which contain total of 1630 consensus nodules, in which 18 are highly suspicious and 10 are pathologically proved cancer.

#### a. Nodule verification

Like other cancers, biopsy for lung cancer is reserved for highly suspicious ones, but unlike other cancer diagnosis, lung nodules are highly prevalent in the screening population and most of the nodules are often indolent. Thereby, most detected lung nodules are left for followup without immediate biopsy. In our collected cases, only 10 out of 1630 nodules were pathologically proved to be malignant and the rest of the nodules are diagnosed based on clinical impressions. To obtain truth of nodule characteristics, we used disease free follow-up for negative nodule verification and meantime we adopted the consensus method, which is widely used and accepted in the scientific groups for lung nodule verification [10].

To obtain consensus results, three experienced thoracic radiologists have reviewed all the nodules. The review process included nodule identification, verification, and characterization. Such review process was repeated at least once to ensure agreement on nodule identification and characterization. Table 1 lists all fields of a nodule description.

Table 1.

Name	Specifications
Nodule number	Number of Nodules
Nodule size	Measured in x, y axes (mm)
Nodule primary character	solid; non-solid (ground glass); mixed solid and non-solid
Nodule borders	smooth; spiculated; lobulated
Calcifications	absent; present
Location (side)	right lung; left lung
Location (lobe)	Right lung: RUL; RML; RLL Left lung: LUL; LLL
CT image number	
CT series	
Risk level	Probability of malignancy

#### *b. Cases anonymization by honest broker*

To comply with HIPPA regulations, the case collection process was solely conducted by an honest broker, who has no any association with this project. After the cases had been selected, all personal information were removed from the cases and the cases were renamed with study numbers.

#### **Reader Training (task 8)**

Participating radiologists receive an "Instructions for Observers" form for review (Appendix C), and the definition of abnormalities are discussed with each reader prior to both the pilot and main studies. Readers were also trained on the use of our scoring mechanism during training session. To verify that observer performance is not affected by relative unfamiliarity or familiarity with our system, we will compare performance of each radiologist at the beginning, middle, an end of the study once we complete the data collection from the pilot study.

#### **Perform Pilot Study (task 9)**

The pilot study was organized as a retrospective study of 108 nodules in 30 cases. Six radiologists, 4 experienced radiologists and 2 fellows, have participated the study. The reading data has been collected and is being analyzed for the performance. This will provide an opportunity to further refine other aspects of the definitive study.

#### **KEY RESEARCH ACCOMPLISHMENTS**

- Developed the mechanisms for a real-time stereographic display for volumetric datasets of lung CT images
- Developed study software for investigating observer performance on stereo display and other commonly used displays for lung CT images
- Developed 3D geometric projection algorithms and transparency-contrast models for compositing of stereo images from volumetric lung CT data
- Collected 290 cases, which include 1630 nodules with 28 that are highly likely as malignancy.
- Trained readers for performing observer performance study-
- Performed the pilot study and collected the data for further analysis

#### **REPORTABLE OUTCOMES**

Peer reviewed paper

**Stereo CT image compositing methods for lung nodule detection and characterization.** *Academic Radiology*, 2005 (in print).

Abstract:

**Real-time stereographic display of volumetric datasets in radiology.** *SPIE, Electronic Imaging*, 2006 (accepted).

Grant application:

**Optimizing MDCT display for detection and diagnosis of pulmonary embolism.** Summated to NIH, June 1, 2005.

**Real-time stereo projection and display for 3D radiographic data.** Submitted to NIH, June 17, 2005.

**Real-time interactive display for virtual endoscopy.** Submitted to NIH, October 19, 2005.

## CONCLUSIONS

Our primary objective is to determine whether a stereoscopic display concept has potential for improving the efficiency and accuracy of chest CT for lung cancer screening. In this progress period, our main tasks were to develop algorithms, software infrastructures and to prepare hardware and study cases, which are all necessary for the study.

Mainly, we have investigated and developed algorithms to generate stereo image pairs from volumetric chest CT images. More specifically, we have used combined models of geometric transformation and transparency-contrast for developing compositing methods that were specially tailored to stereo image pairs from lung CT images. For preparing the study, a software was developed to include the functionalities needed for the observer performance study. In addition, we have built a display workstation that can stereoscopically display chest CT images in real-time, with mechanisms for various user interactive actions.

The important issue we have addressed in this progress period is the optimal rendering methods for nodule detection in lung cancer screening with stereographic display. Choosing a compositing method that is optimal for a particular task, lung nodule in our case, is the key decision in optimizing stereographic displays. Our results indicate that distance-weighted MIP may be a better choice for lung nodule detection in stereo lung CT images for its high local contrast and partial preservation of geometric information, whereas compositing by means of distance-weighted averaging is preferable for nodule characterization. The relative clinical value of these compositing methods will be evaluated in the upcoming data analysis and the main study.

## REFERENCES

1. Greenlee RT, Murray T, Bolder S, et al. Cancer statistics, 2000. *CA Cancer J Clin* 2000; 50:7-33.
2. Ries LAC, Elnsner MP, Kosary CL, et al. SEER: cancer statistics review, 1973-1997. Bethesda, MD: National Cancer Institute, 2000.
3. van Klaveren RJ, Habbema JDF, Pedersen JH, et al. Lung cancer screening by low-dose spiral computed tomography. *Eur Respir J* 2001; 18:857-866.
4. Flehinger BJ, Kimmel M, Melamed M. The effect of surgical treatment on survival from early lung cancer. *Chest* 1992; 101:1013-1018.
5. Sobue T, Suzuki T, Matsuda M, et al. Survival for clinical stage I lung cancer not surgically treated. Comparison between screen-detected and symptom-detected cases. *Cancer* 1992; 69:685-692.
6. Miettinen OS. Screening for lung cancer. *Radiol Clin North Am* 2000; 38:479-486.
7. Anderson BL. Stereoscopic surface perception. *Neuron* 1999; 24:919-928.
8. Anderson BL. The role of occlusion in the perception of depth, lightness, and opacity. *Psychol Rev.* 2003; 110:785-801.
9. Erickson BJ, Rettmann DW. A method for rapid computation of maximum intensity projection images. *J Digit Imaging* 1997; 1093 Suppl 1:207-8.
10. Lori E. Dodd, Robert F. Wagner, Samuel G. Armato, III, Michael F. McNitt-Gray, Sergey Beiden, Heang-Ping Chan, David Gur, Geoffrey McLennan, Charles E. Metz et al. Assessment methodologies and statistical

issues for computer-aided diagnosis of lung nodules in computed tomography: contemporary research topics relevant to the lung image database consortium. Acad Radiol. 2004 11:462-75.

## **APPENDICES**

### **Appendix A**

Peer reviewed paper: Stereo CT Image Compositing Methods for Lung Nodule Detection and Characterization.

### **Appendix B**

Abstract: Real-Time Stereographic Display of Volumetric Datasets in Radiology.

### **Appendix C**

Instructions for Observers.

## Appendix A

### Stereo CT Image Compositing Methods for Lung Nodule Detection and Characterization

Xiao Hui Wang, Walter F. Good, Carl R. Fuhrman, Jules H. Sumkin, Cynthia A. Britton, Saraswathi K. Golla

Department of Radiology, University of Pittsburgh,

#### ABSTRACT

**Rationale and Objectives** Stereographic display has been proposed as a possible method of improving performance in reading CT exams acquired for lung cancer screening. Optimizing such displays is important, given the large volume of image data that must be evaluated for each of these exams. This study was designed to explore certain tradeoffs between rendering methods designed for the stereo display of CT images.

**Materials and Methods** Stereo CT image compositing methods, including distance-weighted averaging, distance-weighted Maximum Intensity Projection (MIP) and conventional MIP, were applied to lung CT images, and compared for lung nodule detection and characterization.

**Results** The Jonckheere test indicated that there was a statistically significant ( $p < 0.01$ ) increase in contrast among the three compositing methods. The Wilcoxon-Mann-Whitney test showed significant differences in contrast between distance-weighted averaging and conventional MIP ( $p < 0.01$ ) and between averaging and distance-weighted MIP ( $p < 0.05$ ), but not between distance-weighted MIP and conventional MIP ( $p > 0.05$ ). The conventional MIP compositing was found to provide the highest image contrast but produced ambiguities in local geometric detail and texture while the averaging resulted in the lowest contrast but preserved geometric detail. Distance-weighted MIP partially recovered geometric information, which was lost in the images composited with conventional MIP.

**Conclusion** Our results indicate that distance-weighted MIP may be a better choice for nodule detection in stereo lung CT images for its high local contrast and partial preservation of geometric information, while compositing by distance-weighted averaging is preferable for nodule characterization. The relative clinical value of these compositing methods needs to be further evaluated.

#### INTRODUCTION

Lung cancer is a leading cause of cancer death in both men and women in the United States [1], [2]. It has been shown that early detection and treatment can effectively reduce mortality from most types of lung cancers [3], [4], [5], [6]. In several large lung cancer screening trials, low-dose helical computer tomography (CT) has proven to be an effective tool for lung cancer screening with superior sensitivity (80 ~ 90%) for early detection, compared to other methods (e.g., chest radiographs with about 23% sensitivity and sputum cytology with 10 ~ 20% sensitivity) [3], [7], [8], [9], [10]. Despite the advantages of using CT as a screening tool for lung cancer, current methods for displaying and interpreting chest CT data are inefficient and inadequate.

At present, the two most common viewing methods employed by radiologists for interpreting these studies involve either reading individual images in a sequential slice-by-slice mode, or viewing thicker slabs comprised of multiple sequential slices projected onto a 2D display. The slice-by-slice method makes it necessary for radiologists to mentally reconstruct 3D information represented in sequential 2D slices in order to differentiate between nodules and linear structures, such as blood vessels, passing through the slices. In addition, the signal-to-noise ratio in single slices may be too low for subtle lesions to be reliably detected.

The use of thicker slabs, obtained by combining thin slices and then projecting this volume onto a 2D display, partially solves these problems but introduces other issues. The thicker the volume being projected, the more likely it is that the superimposed tissues in the projection will result in ambiguities in identifying structures within the projected volume. Furthermore, if slabs are projected by some form of averaging of all voxels projected onto a pixel, the contrast of small nodules may be reduced and this can result in a corresponding reduction in detection performance [11]. As combined slices become thicker by adding more of the originally acquired thin slices the

contrast of smaller nodules, which often are visible on only one or two thin slices, may be reduced by averaging their voxel values with voxel values in slices not containing the nodules.

Over the last decade, maximum intensity projection (MIP) has gained extensive attention for its effectiveness in projecting thicker volumes of CT data, especially angiographic image data [12][13]. This method was originally introduced to overcome the contrast reduction associated with averaging methods and has been studied extensively for this purpose [11]. MIP orthogonally projects the volume of the combined slices onto a 2D display by using the maximum pixel intensity along each ray of the projection. In cases where the object being sought is brighter than superimposed tissues, then the object will be visible in the MIP image. While MIP can improve contrast in volumes that are not too thick, as the thickness of the volume increases the probability that some overlying tissue will have a higher voxel value increases, and this can reduce contrast in MIP images.

MIP is commonly used in procedures requiring the visualization of vascular structures because of its ability to clearly delineate bright objects overlaying a darker background, without significant loss of contrast. In general, MIP displays provide a mechanism for observers to specify the number of individual slices to be combined to form each thick slab, and then enable the observer to move this virtual slab through the data volume.

While such a rendering technique provides no information of depth or of the geometrical relationships between structures (i.e., tissue superposition), albeit the appearance of 3D projections, it does reduce the number of images that must be viewed in order to cover the entire 3D volume. However, the images it produces are, in principle, in conflict with plausible psychophysical transparency/brightness and geometric vision models. Note that, in order to make it possible for observers to appreciate the 3D structure of displayed volumes, these displays sometimes allow the volume to be continuously rotated, though it is known that this kind of image motion actually reduces the effective image resolution as perceived by viewers.

It is likely that higher resolution CT imaging, which will produce more and thinner slices, will be adopted for lung cancer screening in the future, and this will exacerbate problems associated with large data volumes as well as those due to limited signal-to-noise ratios in single slices. If helical CT is to eventually be used for screening for lung nodules, as many have suggested [14], [15], then the efficiency and accuracy of the interpretation process must be increased.

We have proposed the use of stereoscopic 3D displays for reading lung CT images as a possible means to alleviate the aforementioned problems, in hope that this will increase both efficiency and detection performance beyond what can be achieved with other display methods [16], [17]. Such displays, which have the potential to provide more natural representations and volume-based views of structures for viewers having normal binocular vision, have been studied in the past for the display of medical images under various circumstances but, due to technical limitations (e.g., computational power, display technology), these methods have not been widely adopted. However, the current trend toward acquisition of large 3D datasets combined with improvements in the relevant technologies for stereographic display make it prudent to reconsider the potential role of these displays for radiology, at the present time.

Lung CT images are well suited for stereo viewing because, by making air transparent, the sparsely distributed lung tissues of interest (e.g., vessels, airways and nodules) can be easily visualized. Stereoscopic displays have the potential to increase efficiency and signal-to-noise ratios by enabling the display of thicker tissue volumes but they do not introduce the tissue superposition ambiguities that are often associated with a monoscopic presentation of thicker tissue volumes.

For CT data to be displayed stereoscopically, a 3D dataset must be projected onto two views, corresponding to observers' left and right eyes, using a geometric perspective transformation which projects rays through the 3D volume onto individual pixels. This process produces images that simulate what each eye would see if the viewer were looking directly at the 3D dataset. The algorithm that calculates a pixel value from intensity values along a ray, a process often referred to as compositing, determines contrast in the final projected image. Choosing a compositing method that is optimal for a particular task is the key decision that must be addressed in optimizing stereographic displays.

Compositing methods are generally subdivided into those that are related to volume rendering (i.e., methods capable of showing internal structure) and those based on surface rendering. Volume rendering is the most appropriate method for nodule detection in lung CT images, due to its ability to represent internal voxels and to the fact that no segmentation of surfaces, which could introduce artifacts, is required. Within the general paradigm of volume rendering, there are three compositing methods that appear to have some applicability to rendering chest CT data. These include distance-weighted averaging, conventional MIP and distance-weighted MIP.

For most applications, averaging voxel values along rays within the projected volume (i.e., averaging several CT slices to create a thicker image), with or without some form of distance-weighting, is the most commonly used method for compositing stereo volumetric images from individual slices, owing to its preservation of the internal properties of objects. The drawback of the averaging method, as discussed above, is the decrease in contrast of small objects with increasing volume.

Because of its ability to largely solve the contrast problem in many situations, MIP has been widely adopted for the monoscopic display of thicker slabs. However, it is not *a priori* clear that MIP is suitable for stereo compositing because of its inability to preserve the local geometric features and texture of objects and, to a large extent, it is this local information that is required for stereopsis. To achieve stereopsis from two views, a viewer needs to detect corresponding features in each view and to determine the relative geometric disparity between those features. Features that appear in one view (i.e., are a maximum along projections onto the view) may not be represented in a different view if they are not of maximum intensity along a projection for that view, and such features may provide misleading geometric disparity information. This causes small bright objects to have a specular appearance. However, MIP does preserve the presence, but not the exact geometry, of sparsely distributed clusters of bright voxels when they are viewed against a darker background, which is essentially the situation that usually occurs when a nodule is displayed in a thick slab from axial CT slices of the lung. For these reasons, images produced by MIP are, in principle, in conflict with plausible psychophysical transparency/brightness and geometric vision models.

Distance adjusted MIP is an attempt to combine conventional MIP with a psychophysically plausible depth cue, while retaining the contrast advantages of MIP. In this method, the brightness of voxels is reduced as a function of their depth within each projected volume. Brightness as a function of depth is a cue that most individuals subconsciously use all the time. In viewing objects in any transparent medium that has a constant optical density per unit of thickness, the brightness of an object will vary according to an exponential function of depth. MIP displays using this sort of depth cue vary the brightness throughout slabs as they are moved through the tissue volume to provide a plausible simulation of the optical properties corresponding to uniform optical density. This process has the added benefit for MIP that it can change the relative brightnesses of voxels based on the position of slabs containing the voxels, which can improve the detectability of objects that are similar in brightness to their backgrounds.

These various alternatives for compositing have not been previously compared in the context of nodule detection in chest CT, and the degree to which the concerns mentioned above could affect tasks such as nodule detection in lung CT images is unknown. This paper explores these compositing methods with the goal of identifying methods suitable for the stereographic display of lung CT for the purpose of nodule detection.

## **MATERIALS AND METHODS**

### **1. Lung CT images and nodule verification**

Ten sets of lung CT images, each containing a consensus-proven solitary lung nodule, were used in this study. For each image set, stereo image pairs were projected using four compositing methods including distance-weighted averaging, MIP and two versions of distance-weighted MIP. The images were displayed with window/level setting of 1800/-600 for MIP images and 1500/-600 for averaging. Contrast and nodule characteristics were compared between these compositing methods.

### **1.1. Lung CT images**

Helical CT images were obtained from a low-dose CT lung cancer screening project conducted in the Medical Center, University of Pittsburgh. The CT cases were performed on a LightSpeed Plus multislice CT scanner (GE medical Systems, Milwaukee, WI) using X-ray tube current of 40-mA, voltage of 140-kVp and 0.5-mm pitch. The images were acquired in the axial plane and reconstructed to a thickness of 2.5 mm/slice with GE standard convolution software for lung tissue. The pixel size in each slice is 0.75-mm  $\times$  0.75-mm.

### **1.2. Nodule verification**

All the nodules used in this paper were identified, verified, marked and characterized by three experienced radiologists. The verification process was repeated at least one time to ensure agreement on the nodule identification and characterization. Table 1 lists the nodules and their properties.

## **2. Stereo compositing methods**

The voxel shape in the CT images used in this study was nonisotropic in that images had been reconstructed to a larger thickness in z direction (i.e., slice thickness of 2.5-mm) than in x and y directions (pixel dimension: 0.75  $\times$  0.75-mm). To approximate isotropic voxels, three slices were created by trilinear interpolation between each pair of adjacent CT slices. Consecutive slices, including CT and interpolated slices, within a given volume were used for generating a stereo pair.

In the conventional geometric perspective transformation that was used to compose left-eye and right-eye image pairs, we adopted an interpupillary distance of 6.5-cm, a viewing distance (the distance between eyes and the screen) of 45-cm and a display area of 25-cm  $\times$  25-cm. The perspective transformation was symmetrical, based on the assumption that a viewer is centered in front of the screen.

Each set of slices was composited to a stereo pair for each of the projection methods. Since the effect of superimposed tissue is different for each of the compositing methods, the characteristics of a projection method depend on the depth of a nodule within a 3D volume. Thus, in order for us to compare the depth-dependence of compositing methods, for each nodule we constructed three volumes with the nodule at different depths in each volume. Specifically, the three volumes were comprised of: 1) precisely those slices that cover the nodule; 2) all slices in the first set plus an additional 3 slices in front of the nodule; and, 3) all slices in the first set plus an additional three slices behind the nodule.

### **2.1. Traditional Compositing by Distance-Weighted Averaging**

For this compositing method we adopted a light emission/transmission/occlusion model that assumed that each voxel emits light in proportion to its brightness when the CT images are displayed at a normal window and level for nodule detection, and that uses distance information (distance weighing factors) to determine the amount of this emitted light that reaches the projection plane.

Specifically, it was assumed that each slice has a fixed optical density that reduces the brightness of slices lying behind it. The total of all distance-weights was equal to one. The ratio of the weights between the last slice (the slice with the largest distance from screen) and the first slice (the slice at screen level) controls level of transparency for a given volume.

We have studied a range of these ratios for lung CT images, and empirically set the ratio to 0.5 in order to achieve a balance between the use of brightness weighting as a depth cue and the visibility of the back slice. The final value for a voxel is the sum of distance-weighted pixel values in a perspective transformation ray. The detailed calculations were described in references [16] and [17].

### **2.2. Stereographic MIP Compositing**

This compositing method uses a perspective projection in which the maximum value along each ray is used as the projected value. Because the projected voxels may be different between the stereo views, it is not generally possible for an observer's vision system to unambiguously match corresponding points between the two views. This may cause small objects, such as lung nodules to have a speckled appearance. Thus, this method is not *a priori* suitable

for stereo projection. In practice, we have found that the ambiguity in matching corresponding points between views primarily affects fine detail and does not interfere with the detection of objects that are comprised of large clusters of bright voxels, though the exact shapes of these objects cannot be unambiguously determined.

### 2.3. Distance-Weighted Stereographic MIP

In an attempt to incorporate a geometric cue common in traditional stereo projection methods, but also preserve the contrast advantage of MIP, we employed a perspective projection in which the maximum along each ray is weighted based on distance. Since MIP only takes one pixel value along a ray, the sum of total weight is irrelevant in this case and therefore, only the maximum (nearest) and the minimum (farthest) weights were empirically determined. Based on transparency/occlusion model, the first slice was weighted as 1, the last slice was weighted as 0.5 and weights for slices between the first and the last were calculated using a geometric sequence, assuming a fixed optical density for each slice.

There are two paradigms for applying distance-weighting to MIP. Voxel values can either be adjusted by distance weights prior to acquiring the maximum value along a ray (Distance-MIP), or alternatively, the maximum value can be chosen first and then adjusted by applying the distance-weighting factor (MIP-Distance). In this study, we have tried both strategies and a comparison was made based on image appearances and contrast measurements.

### 3. Contrast analysis

The boundaries of the identified nodules were manually marked on CT slices. The background included the area of 20-mm from the nodule boundary in x, y and z directions. Local contrast was measured using Michelson Contrast measure  $C_m$ , with local maximum intensity  $L_{max}$  and minimum intensity  $L_{min}$ ,

$$C_m = \frac{L_{max} - L_{min}}{L_{max} + L_{min}}.$$

The one-tailed Jonckheere test was used for testing for a significant trend of increasing contrast for the group of three compositing methods as ordered in the statement of the hypothesis. The one-tailed Wilcoxon-Mann-Whitney Test was used for testing the significance of difference in contrast measures between averaging and conventional MIP, between averaging and distance-weighted MIP, and between distance-weighted MIP and conventional MIP.

## RESULTS

We have compared averaging, MIP and distance-weighted MIP applied to various nodule types, sizes and locations. Figure 1 illustrates three sets of nodules to show typical examples resulting from the three stereo compositing methods. Figure 1A shows a solid nodule with smooth border, and Figures 1B and 1C show nonsolid nodules with spiculated borders. As is shown in Figure 1, MIP and distance-weighted MIP produced higher local contrast than compositing by averaging, in all subsets. If the area surrounding a nodule contains dense structures, such as bone in this case, a nodule can be camouflaged by, or blended into, the background when stereo pairs are rendered with conventional MIP, as shown in Figure 1B and Figure 1C. This camouflage effect is less noticed in the distance-weighted MIP images.

Local contrast measures for 10 nodules with different compositing methods are listed in the Table 2, where each cell has 3 sets of Michelson Contrast numbers. Two numbers in a set are for the left and right images in a stereo pair, and the first set of numbers are from the subset of images containing a nodule, the second set of the numbers are from the images containing the nodule plus extra front slices and the third set of the numbers are from the images containing a nodule plus extra back slices. In general, conventional MIP and distance-weighted MIP (both MIP-Distance and Distance-MIP) produced higher contrast measures compared to the averaging method. The contrast measures from MIP method are fairly constant in all slab thickness used in this study, while the averaging method resulted in decreasing contrast as slab thickness increased. There is a statistical significant ( $p < 0.01$ ) of ordered contrast change (averaging, distance-weighted MIP, conventional MIP) among the three compositing methods as measured by Jonckheere test. Also notice that the MIP-Distance approach, in general, had slightly higher average contrast

measures than the Distance-MIP approach. When comparing contrast between the compositing methods, the one-tail Wilcoxon-Mann-Whitney Test indicated that there was a significant difference between averaging and distance-weighted MIP (either MIP-Distance approach or Distance-MIP approach,  $p < 0.05$ ), between averaging and conventional MIP ( $p < 0.01$ ) in all three compositing thicknesses. There was no statistically significant difference in contrast measure between distance-weighted MIP and conventional MIP in all three compositing thicknesses ( $p > 0.05$ ), except one pair, which was the difference between Distance-MIP and conventional MIP applied to the subgroup of nodule with three front slices ( $p = 0.0375$ ).

Finally, we have compared the three compositing methods visually for nodule characterization. As shown in the Figures 1B and 1C, the spiculated nodule border is clearly visible in all stereo pairs composited with averaging method, while this characteristic is not preserved in some of the stereo pairs composited with conventional MIP method, especially those composited from thicker slabs. Distance-weighted MIP partially overcomes the problem of conventional MIP, and spiculated borders are still visible in the thicker slabs. As for the smooth border we observed similar phenomenon. The geometric relationship is well presented with gradient changes in intensities along the smooth border of the nodule (Figure 1A) in the stereo pair composited with averaging method. The same nodule is displayed with lack of geometric fidelity, as shown by the sharp edge of the smooth border in the stereo pair composited with conventional MIP.

## DISCUSSION

Previously, we have shown that stereoscopic display for lung CT images can dramatically improve display efficiency and lung nodule visibility, relative to conventional slice-based displays. In this present study, we have further investigated the effects of several commonly used compositing methods on nodule representation in stereo CT images.

The results from this study, as well as from others, have shown that unlike averaging methods, which sacrifice contrast in order to take account of each voxel in a volume, the conventional MIP method is able to retain contrast in cases where the object being viewed includes voxels that are brighter than the superimposed tissue. As applied to the task of lung nodule detection, despite a lack of geometric fidelity, the conventional MIP images generally produce high local contrast that separates a nodule from its background, and therefore enhances detection performance.

The improvements in nodule visibility with the MIP method, however, do not apply in certain cases in lung CT images. For a nodule to be detected with conventional MIP, it must contain some voxels that are brighter than its background. The case of a nodule overlying a rib is a particular concern though it occurs relatively infrequently in projections of axial slabs, unless the nodule is very close to a rib or the slab being viewed is relatively thick. Most voxels in such a nodule will not be as bright as voxels in the rib and the nodule may be almost invisible. Examples from this study (MIP images in Figures 1B and 1C), in which the nodules are almost indiscernible when they are close to bone tissue, have demonstrated this effect.

This same potential problem occurs in monoscopic MIP displays that are already in wide use. The situation is actually somewhat improved in the case of stereo viewing. Traditional MIP employs an orthogonal projection, the rays of which do not change relative to the 3D volume as a slab is moved in the axial direction. This means that when a voxel of a rib and a voxel of a nodule fall on the same ray of a projection, then the two voxels will always be superimposed when both are contained within a slab. The stereographic projections we are using involve two perspective transformations for each axial position of a slab. The angles of rays passing through a nodule, in each of these projections are different so that if two voxels are superimposed along one ray they will not be along the other. Furthermore, as a slab is moved in the axial direction, the orientation of a projection ray passing through a particular voxel changes continuously, so that the sets of superimposed voxels change continuously. Thus, if a slab is moved slightly, an obscured nodule is more likely to become visible with stereographic projection as opposed to monoscopic MIP.

One benefit of the distance weighted MIP projection is that it can reduce the brightness of the background. As the position of a slab is changed, the relative brightness weighting factors between voxels at different axial positions will

change and, in many instances, there will be an axial position where a nodule will appear brighter than a rib and this can increase the likelihood that an obscured nodule becomes visible.

Segmenting the ribs and spine can theoretically reduce this problem, but that process may generate its own artifacts. Segmentation would involve some sort of surface detection, and if the surfaces were perfectly smooth, that should not present any difficulties. However, any realistic surface detection algorithm must differentiate between roughness of the surface and nodules lying near the surface. If a computer could do this reliably then there would be no need for the radiologist to view the images. Consequently, we are particularly concerned about the risks of segmentation in precisely those cases where it could be of potential value.

As described in the methods, we have tried two different ways for distance-weighted MIP compositing, the Distance-MIP approach and the MIP-Distance approach. The two approaches produced slightly different results due to the fact that different maximum intensities were chosen. For distance-MIP, the maximum value  $I_{max}$  is dependent on weight distribution in  $j$  elements  $I_j$ ,

$$I_{max} = \max(I_1 w_1, I_2 w_2, I_3 w_3, \dots, I_j w_j).$$

If weight distribution,  $w_1, w_2, w_3, \dots, w_j$ , drops fast, weighted values away from the front are greatly reduced, and it is more likely that values nearer the front will be chosen. In this case, the final image may represent only a few slices in the front, and volume information could be lost. In this study, that effect was not apparent because of the relatively slow change in the weighing factors. For the MIP-Distance approach, although it may not necessarily have the maximum intensity in the final images as might be the case if a chosen voxel had a large reduction in intensity because it was located in the back, it does take into account the entire volume and produces contrast generally as good as that with Distance-MIP. An example is shown in Figure 1B (3 slices + nodule) in which the geometric relationship was better preserved in the images rendered with MIP-Distance compositing compared to Distance-MIP compositing. For the purpose of detection and diagnosis, the MIP-Distance approach may be preferred to the Distance-MIP approach.

Our results indicate that both versions of distance-weighted MIP partially recover geometric information lost in conventional MIP, by incorporating a distance cue into the compositing. As shown in the Figure 1, distance-weighted MIP reveals the nodule within the bone area (Figures 1B and 1C), where the same nodule is not easy to detect in the conventional MIP projection. However, the distance-weighted MIP had image contrast nearly equivalent to that produced by the conventional MIP method. Overall, distance-weighted MIP retained most of the contrast of MIP, while improving geometric fidelity.

In addition to detection, the nodule characteristics are essential and critical for clinically differentiating benign from malignant. Although the conventional MIP is superior for detection, it was outperformed by the distance-weighted averaging method in terms of characterization, as can be seen in our results. The lack of fidelity in nodule shape and geometric representation, in the conventional MIP images, are attributed to the nature of MIP compositing, in which the two views may be based on projections of different voxels. The averaging method, on the other hand, has been shown in this study to faithfully retain the characteristics of the nodules, including structural, spatial and geometric information. This can be observed in all nodules tested in this study.

Because nodules must be detected before they can be characterized, and we have shown a tradeoff between contrast for detection and geometric fidelity for characterization, we believe that the use of two separate stereoscopic display modes is both desirable and feasible. First, the image data should be displayed using some form of distance-weighted MIP to maximize detection performance. Once a nodule has been detected, the thickness of the displayed volume can be adjusted so as to include only those slices that contain the nodule, and this volume can be displayed using an averaging compositing method in order that the nodule can be more accurately characterized.

Unfortunately, while monoscopic approaches to 3D display can be appreciated by most individuals, there is a significant variation across the population in the ability to achieve stereopsis [18]. It has been reported that 2% to 4% of individuals are stereopsis blind and another 10% to 15% have a stereopsis deficiency in the sense that they have difficulty deriving 3D information from random-dot stereograms. Much of the stereopsis impairment, reflected in

these numbers, has been attributed to strong uncorrected astigmatism [18]. This would seem to limit the value of stereo display to the subpopulation having normal binocular vision. This kind of limitation is not unprecedented in radiology – colorblind radiologists would likely have difficulty taking advantage of the benefits of using color on a PET display, for example, and previously, medical student applicants for a stereo X-ray fluoroscopy training program have been prescreened using random-dot stereograms. Nevertheless, for the majority of radiologists, stereographic methods may provide a more natural way for them to perceive the spatial relationships in 3D volumetric datasets, and those radiologists who are unable to achieve stereopsis would be able to continue to reading from traditional monoscopic displays or employ other means of representing 3D data.

There is also a concern that even individuals who can achieve stereopsis on surface rendered images will have difficulty seeing volume rendered images in stereo, though there is no direct evidence of this. In any event, in the scenario we are studying with respect to stereographic projection of the lung, the objects whose positions we are trying to clarify are small relative to the lung volume and tend to be sparsely distributed. In the detection task, it is not as important that we see the internal structures of the objects in stereo, as it is that we see the relative positions of the objects in stereo. We could achieve our goals by surface rendering the interior of the lung, but as mentioned above, that kind of calculation requires that rather intelligent emulation of the mental processing typical of radiologists, be performed in software. This has the risk of introducing other artifacts, and is not necessary to solve the detection problem.

The advantage of applying stereoscopic technique over other 3D rendering techniques for medical 3D data display is that stereo display employs a mechanism naturally used by human visual system for detecting and characterizing objects. By presenting data in a volume-based stereoscopic format, radiologists' efficiency and accuracy in interpreting CT images may be significantly improved. Although the actual value of stereo display for lung cancer screening is not yet known, it was the intention of this study to begin to investigate methods for achieving optimal image quality in anticipation of future observer performance studies aimed at measuring the efficacy of stereo displays for chest CT. It is noted that this study has involved a small sample size of test sets, and a much larger study would be required to clarify all differences between the compositing methods.

## ACKNOWLEDGEMENTS

This work is sponsored in part by grant CA80836 from the National Cancer Institute, National Institutes of Health, and also by the US Army Medical Research Acquisition Center, 820 Chandler Street, Fort Detrick, MD 21702-5014 under Contract DAMD17-02-1-0549 and contract PR043488. The content of the contained information does not necessarily reflect the position or the policy of the government, and no official endorsement should be inferred.

## References

1. Greenlee RT, Murray T, Bolden S, et al. Cancer statistics, 2000. *CA Cancer J Clin* 2000; 50:7-33.
2. Ries LAC, Eisner MP, Kosary CL, et al. SEER: Cancer statistics review, 1973-1997. NCI 2000.
3. van Klaveren RJ, Habbema JDF, Pedersen JH, et al. Lung cancer screening by low-dose spiral computed tomography. *Eur Respir J* 2001; 18:857-866.
4. Flehinger BJ, Kimmel M, Melamed M. The effect of surgical treatment on survival from early lung cancer. *Chest* 1992; 101:1013-1018.
5. Sobue T, Suzuki T, Matsuda M, et al. Survival for clinical stage I lung cancer not surgically treated. Comparison between screen-detected and symptom-detected cases. *Cancer* 1992; 69:685-692.
6. Miettinen. OS. Screening for lung cancer. *Radiol Clin North Am* 2000; 38:479-486.
7. The American Society of Cytopathology, Cytopathological Practice Committee, "Nongynecological cytology practice guidelines." The American Society of Cytopathology, <http://www.cytopathology.org/guidelines/nongynecologicalxi.php>.

8. Jett JR, Midthun DE. Screening for lung cancer: current status and future directions. *Chest* 2004; 125(5 Suppl):158S-162S.
9. Kawahara M. Screening for lung cancer. *Curr Opin Oncol* 2004; 16:141-145.
10. Diederich S, Thomas M, Semik M, et al. Screening for early lung cancer with low-dose spiral computed tomography: results of annual follow-up examinations in asymptomatic smokers *Eur Radiol* 2004; 14:691-702.
11. Brown DG, Riederer SJ. Contrast-to-noise ratios in maximum intensity projection images. *Magn Reson Med* 1992; 23:130-137.
12. Napel S, Rubin GD, Jeffrey RB, Jr. STS-MIP: a new reconstruction technique for CT of the chest. *J Comput Assist Tomogr* 1993; 17:832-838.
13. Calhoun PS, Kuszyk BS, Heath DG, Carley JC, Fishman EK. Three-dimensional volume rendering of spiral CT data: theory and method. *Radiographics* 1999; 19:745-764.
14. Gohagan J, Marcus P, Fagerstrom R, et al. Baseline findings of a randomized feasibility trial of lung cancer screening with spiral CT scan vs chest radiograph: the Lung Screening Study of the National Cancer Institute. *Chest* 2004; 126:114-121.
15. Armstrong P, Husband JE, Holemans JA. Population screening for lung cancer. *Hosp Med* 2004; 65:404-411.
16. Wang XH, Good WF, Fuhrman CR, et al. Stereo Display for Chest CT. *Proc SPIE* 2004; 5291:17-24.
17. Wang XH, Good WF, Fuhrman CR, et al. Projection Models for Stereo Display of Chest CT. *Proc SPIE* 2004; 5367:676-686.
18. Julesz B. Foundations of Cyclopean Perception. The University of Chicago Press, 1971; page 270.

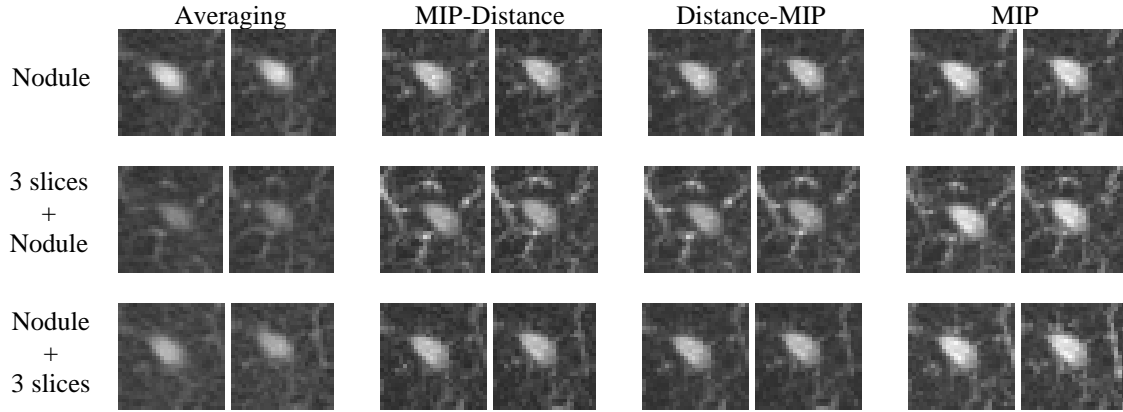
Table 1. Nodule information.

Nodule #	Size (mm <sup>2</sup> )	Border	Characteristic
1	4×2	Smooth	Solid
2	8×6	Spiculated	Non-solid
3	10×7	Spiculated	Solid
4	7×7	Spiculated	Non-solid
5	6×4	Speculated	Mixture of solid and non-solid
6	6×5	Spiculated	Solid
7	5×4	Smooth	Mixture of solid and non-solid
8	10×9	Spiculated	Mixture of solid and non-solid
9	6×5	Smooth	Mixture of solid and non-solid
10	6×5	Smooth	Mixture of solid and non-solid

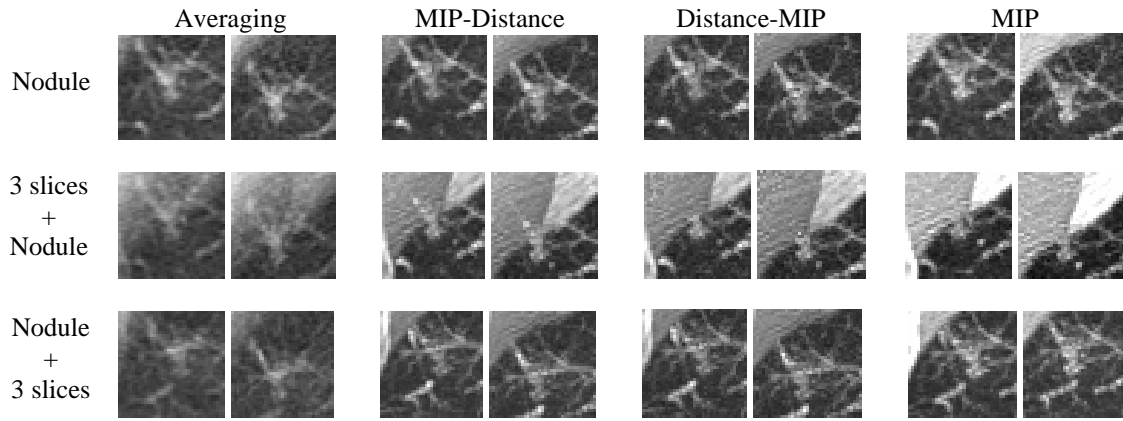
Table 2. Contrast measurements with Michelson Contrast Measure. Three sets of measurements in each cell are the stereo pairs (left and right) composited from the nodule slices, the nodule slices with 3 front slices, and nodule slices with 3 back slices, respectively.

Nodule #	Averaging	MIP-Distance	Distance-MIP	MIP
1	0.82 / 0.84 0.73 / 0.71 0.76 / 0.74	0.85 / 0.85 0.81 / 0.79 0.81 / 0.81	0.84 / 0.85 0.81 / 0.77 0.80 / 0.80	0.85 / 0.86 0.84 / 0.83 0.81 / 0.83
2	0.84 / 0.84 0.79 / 0.83 0.79 / 0.78	0.88 / 0.86 0.82 / 0.87 0.84 / 0.85	0.84 / 0.84 0.79 / 0.83 0.87 / 0.85	0.89 / 0.88 0.85 / 0.90 0.87 / 0.85
3	0.89 / 0.84 0.82 / 0.80 0.87 / 0.80	0.90 / 0.86 0.89 / 0.89 0.87 / 0.85	0.91 / 0.85 0.90 / 0.88 0.87 / 0.80	0.94 / 0.89 0.90 / 0.89 0.90 / 0.88
4	0.91 / 0.92 0.87 / 0.87 0.89 / 0.88	0.92 / 0.93 0.89 / 0.88 0.91 / 0.92	0.92 / 0.93 0.90 / 0.88 0.90 / 0.91	0.94 / 0.95 0.90 / 0.91 0.93 / 0.94
5	0.82 / 0.84 0.77 / 0.80 0.79 / 0.83	0.85 / 0.87 0.82 / 0.84 0.83 / 0.87	0.86 / 0.89 0.81 / 0.84 0.82 / 0.87	0.88 / 0.91 0.85 / 0.86 0.85 / 0.88
6	0.91 / 0.93 0.90 / 0.89 0.89 / 0.88	0.97 / 0.96 0.93 / 0.92 0.92 / 0.92	0.96 / 0.96 0.93 / 0.92 0.93 / 0.93	0.99 / 0.98 0.98 / 0.96 0.98 / 0.98
7	0.76 / 0.91 0.75 / 0.79 0.73 / 0.77	0.82 / 0.91 0.79 / 0.80 0.76 / 0.79	0.78 / 0.90 0.79 / 0.79 0.76 / 0.77	0.87 / 0.96 0.81 / 0.85 0.77 / 0.83
8	0.93 / 0.93 0.90 / 0.90 0.91 / 0.92	0.96 / 0.96 0.94 / 0.95 0.92 / 0.91	0.96 / 0.95 0.94 / 0.94 0.94 / 0.94	0.99 / 0.99 0.98 / 0.99 0.98 / 0.97
9	0.78 / 0.80 0.72 / 0.73 0.75 / 0.75	0.81 / 0.86 0.80 / 0.80 0.82 / 0.84	0.80 / 0.82 0.79 / 0.80 0.86 / 0.86	0.87 / 0.88 0.82 / 0.82 0.86 / 0.86
10	0.92 / 0.93 0.83 / 0.82 0.85 / 0.84	0.93 / 0.94 0.86 / 0.91 0.91 / 0.91	0.93 / 0.94 0.86 / 0.84 0.91 / 0.90	0.96 / 0.96 0.90 / 0.91 0.92 / 0.91

Figure 1.  
A.



B.



C.

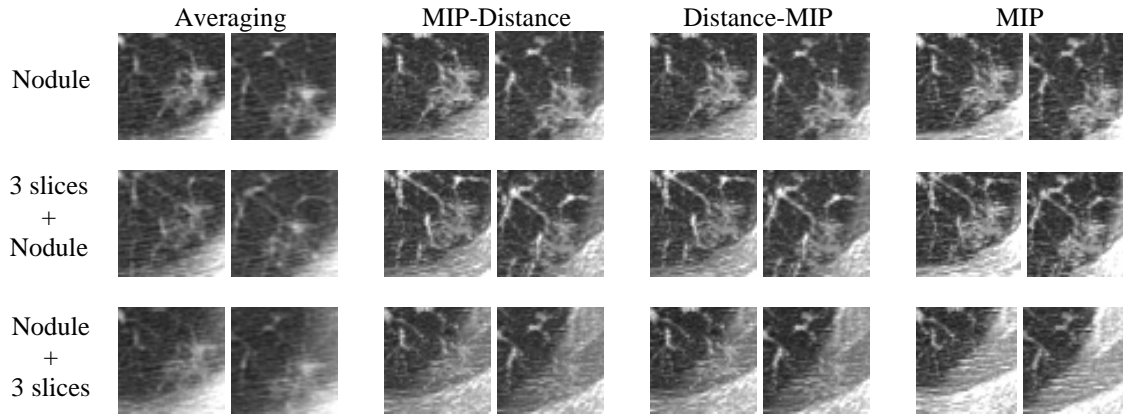


Figure 1. Stereo image pairs of three nodule sets (A., B., and C.). Images of A, B, and C are from nodule #1, nodule #2 and nodule #4, respectively as denoted in the table 1 and table 2. In the row labels of each set, "Nodule" means the images were composited from nodule slices, "3 slices + Nodule" means the images were composited from nodule slices plus 3 front slices, and "Nodule + 2 slices" means the images were composited from nodule slices plus 3 back slices.

## **Appendix B.**

### **Real-Time Stereographic Display of Volumetric Datasets in Radiology**

Xiao Hui Wang, Glenn S. Maitz, J. Ken Leader, Walter F. Good

A workstation for testing the efficacy of stereographic displays for applications in radiology has been developed, and is currently being tested on lung CT exams acquired for lung cancer screening. The system exploits pre-staged rendering to achieve real-time dynamic display of slabs, where slab thickness, axial position, compositing method, brightness and contrast are interactively controlled by viewers. Stereo viewing is by means of shutter-glasses synchronized to a 144 Hz monitor. The system enables viewers to toggle between alternative renderings such as one using distance-weighted ray-casting by maximum-intensity-projection, which is optimal for detection of small features in many cases, and ray-casting by distance-weighted averaging, for characterizing features once detected.

A reporting mechanism is provided which allows viewers to use a stereo cursor to measure and mark the 3D locations of specific features of interest, after which, a pop-up dialog box appears, into which findings can be entered.

In the past, stereo displays have been underutilized in radiology as a result of a perception, which developed prior to the widespread adoption of inherently 3D imaging modalities, that they provide only a minimal benefit to experienced radiologists. Because there is no consensus with regard to the efficacy of stereoscopic displays in radiology, the system's impact on performance is being tested on chest CT exams for lung cancer screening. These exams are uniquely suited for testing the potential of stereographic display methods in radiology. On each slice, radiologists must determine whether small round spots correspond to a vessel passing through the slice or to a cross-section of a nodule – a task that is very dependent on the 3D information in adjacent slices. In addition to this objective study of performance, radiologists' subjective assessments have been solicited for other kinds of 3D exams (e.g., breast MRI). Radiologists' subjective responses to the system have been positive, but objective estimates of changes in performance and efficiency must await the conclusion of our study.

We are in the process of implementing the rendering calculations on the computer's graphics-processing unit so that they can be performed in real time. This will greatly increase the system's flexibility in having users interactively specify views.

## Appendix C.

### Instructions for Observers

**Introduction** – This study is designed to measure the relative performances of different display methods used for detecting nodules in lung CT exams. Its goal is to evaluate any association between display method, performance and efficiency in reading chest CT exams acquired for lung cancer screening.

**Task** – You will be shown a series of lung CT exams and asked to identify, and mark the locations of, features that correspond to possible nodules having sizes  $\geq 3$ -mm. Your confidence as to the likelihood that a detected feature is a nodule, and your assessment of its characteristics, are to be entered into a dialog box that pops up when a feature is marked. All cases will be viewed in one of three display modes on a CRT monitor.

**Definition of a possible nodule** – For the purposes of this study a nodule will be defined as a round opacity, at least moderately well margined and no greater than 3-cm in maximum diameter. This would not include obvious linear scars or nonspecific opacities without definite boundaries. However, marking such abnormalities, and then entering a low rating for likelihood of being a nodule, may be an appropriate response in certain cases. These cases have a relatively high concentration of nodules. There may be more than one nodule in a single case. Other abnormalities may be present, but for the purposes of this study, they should be ignored.

**Display** – The workstation provides for three display modes, though only a single mode will be available during any given reading session. The display modes include: 1) traditional slice-by-slice; 2) MIP display of thick slabs; and, 3) stereo display of thick slabs. In both the MIP and stereo modes, when the slab thickness is set to 1, the displays are equivalent to the slice-by-slice mode.

All user interaction will be through the use of the computer's mouse and a specialized keypad. You will use keypad keys to navigate through slices and to adjust the display's window and level. In the MIP and Stereo display modes, slab thickness and axial position can be controlled through the keypad. The locations of suspected nodules are to be marked by clicking on the displayed image. The mouse is also to be used to answer questions on the dialog box that pops up when a possible nodule is marked. There is no time restriction for evaluating a case. Detailed instructions for each mode are provided below.

### General Instructions for All Display Modes

**Marking the Locations of Possible Nodules** – The locations of possible nodules are to be marked by moving the crosshair cursor over the nodule and left-clicking. A box will be displayed on the image, centered on the marked location. At the same time, a scoring form will pop up on the right hand side of the screen. Once the scoring form has been completed, the box is replaced by a small triangular cue, and it is possible to proceed with the case.

**Measuring Sizes** – The cross-hair cursor measures 1-cm  $\times$  1-cm, relative to the dimensions of the image data, and can be used to estimate the sizes of features, before they are marked. Once a location is marked, a 2-cm  $\times$  2-cm box (with tic marks 5-mm long) is placed around the location while the scoring form is visible, and can be used for estimating sizes.

**Answering Questions on the Scoring Form** – Answer the questions on the scoring form based on your assessment of the marked location. The 1<sup>st</sup> question on the scoring form relates to your subjective estimate of the likelihood that a nodule is present at the marked location; with 0 indicating that you believe there is definitely not a nodule, and 100 indicating that you are certain a nodule is present. The second question, which relates to the likelihood that the nodule is malignant, is to be answered similarly. In both cases, it is important that, as far as possible, you use the entire scale when you express your actual level of confidence for each detection. In particular, do not be excessively dogmatic in the sense of reducing most ratings to yes or no decisions with ratings of 0 or 100%. Such extreme ratings should be reserved for those cases in which your confidence level is, in fact, extremely high. When you have completed the scoring form click on the **OK** button. The scoring form will disappear and the box surrounding the marked location will be replaced by a small triangular cue.

**Showing or Hiding Marked Locations** – Cues identifying the marked locations can be displayed or hidden by pressing either the **Show Marks** or **Hide Marks** buttons on the keypad.

**Changing Answers or Deleting Marked Locations** – Answers for a previously marked location in the current case can be changed, or the marked location deleted, by clicking on the cue identifying the location. A scoring form containing the previous answers will be presented. Answers can be changed or the marked location can be deleted (by clicking **Delete** button).

**Saving Answers and Proceeding to Next Case** – After you have marked all of the locations you consider to be suspicious for a nodule, your answers are to be finalized and recorded by clicking on the **Save Answers and Go To Next Case** button. If there are more cases available to be read in your current reading session, a new case will be presented.

**Terminating a Reading Session** – To terminate the reading session, click on **Exit** in the drop-down **File** menu (upper left corner of screen). We have not specified a fixed number of cases for a reading session. However, the total number of interpretations is fixed, so the more you complete in each session, the sooner you will complete the study.

**Window and Level Adjustment** – The displayed window and level can be adjusted, or set to default values, by using buttons on the keypad as shown in the "Instructions for Keypad" figure.

**Axial Position** – In all display modes, slice position within the dataset can be set by using buttons on the keypad as shown in the "Instructions for Keypad" figure.

### **Specific Instructions for Stereo Display Mode**

**Use of Shutter Glasses** – In the stereo display mode, it is necessary to wear the shutter glasses. The display actually toggles between a left-eye view and a right-eye view of the 3-D data at a rate of 140 Hz. When viewing thicker slices in this mode, these two views will appear to be superimposed on the display if viewed without using the shutter glasses.

**Adjusting Slab Thickness** – Slab thickness can be adjusted by using the blue buttons on the keypad as shown in the "Instructions for Keypad" figure.

**Viewing Original (Unmodified) Image Data** – Viewing data at the minimum slab thickness (1 slice) is equivalent to viewing the data in the slice-by-slice mode.

**Marking Nodule Locations** – When a location is marked on the image, and the scoring form has been completed, a small triangular cue is placed on each visible slice. However, for the purpose of scoring, we assume the cue is attached to the center slice of the slab. Thus, to more accurately identify the position of a nodule in the axial direction when the nodule is detected in a thicker slab, it may be necessary to reduce the thickness of the slab before marking the nodule's location.

**Measuring Sizes** – The crosshair cursor measures 1-cm  $\times$  1-cm, relative to the dimensions of the slice in which it is displayed (middle slice), and can be used to estimate the sizes of features before they are marked. Once a location is marked and the scoring form is visible a box, which is placed around the location, can be used for estimating sizes. The box measures 2-cm  $\times$  2-cm and has 5-mm long tic marks, relative to the dimensions of the middle slice. Because both of these are displayed in the middle slice of thick slabs, they will appear to change size slightly, as slab thickness is changed, to reflect changes in the dimensions of middle slices resulting from the stereo perspective transformation.

**Changing Projection Method** – Two methods for stereo projection – MIP and averaging – are available in the stereo display mode. MIP is the default, and is generally considered to be preferable for detection of nodules, but it does not preserve geometric fidelity. Averaging gives a more accurate representation of geometric detail, but

provides less contrast. We expect that the highest performance will be achieved when stereo projection by MIP is used for detection, and the user switches to projection by averaging only when it is necessary to see the geometric detail more clearly. Clicking on the buttons **Change to MIP Projection** and **Change to Averaging Projection** are used to toggle between these two renderings. Note that the stereo projection method is reset to MIP after each scoring form is completed and when a new case is presented.

### **Specific Instructions for MIP Display Mode**

**Adjusting Slab Thickness** – Slab thickness can be adjusted by using the blue buttons on the keypad as shown in the "Instructions for Keypad" figure.

**Viewing Original (Unmodified) Image Data** – Viewing data at the minimum slab thickness (1 slice) is equivalent to viewing the data in the slice-by-slice mode.

**Marking Nodule Locations** – When a location is marked on the image, and the scoring form has been completed, a small triangular cue is placed on each visible slice. However, for the purpose of scoring, we assume the cue is attached to the center slice of the slab. Thus, to more accurately identify the position of a nodule in the axial direction when the nodule is detected in a thicker slab, it may be necessary to reduce the thickness of the slab before marking the nodule's location.

**Measuring Sizes** – The cross-hair cursor measures  $1\text{-cm} \times 1\text{-cm}$ , relative to the dimensions of the image data, and can be used to estimate the sizes of features, before they are marked. Once a location is marked, a  $2\text{-cm} \times 2\text{-cm}$  box (with tic marks 5-mm long) is placed around the location while the scoring form is visible, and can be used for estimating sizes.